PCCP

Cite this: *Phys. Chem. Chem. Phys.*, 2011, **13**, 10510–10519

www.rsc.org/pccp

PAPER

Adaptive resolution simulation of liquid *para*-hydrogen: testing the robustness of the quantum-classical adaptive coupling

A. B. Poma and L. Delle Site*

Received 13th December 2010, Accepted 17th February 2011
DOI: 10.1039/c0cp02865g

Adaptive resolution simulations for classical systems are currently made within a reasonably consistent theoretical framework. Recently we have extended this approach to the quantum-classical coupling by mapping the quantum nature of an atom onto a classical polymer ring representation within the path integral approach [Poma & Delle Site, *Phys. Rev. Lett.*, 2010, **104**, 250201]. In this way the process of interfacing adaptively a quantum representation to a classical one corresponds to the problem of interfacing two regions with a different number of effective "classical" degrees of freedom; thus the classical formulation of the adaptive algorithm applies straightforwardly to the quantum-classical problem. In this work we show the robustness of such an approach for a liquid of *para*-hydrogen at low temperature. This system represents a highly challenging conceptual and technical test for the adaptive approach due to the extreme thermodynamical conditions where quantum effects play a central role.

I. Introduction

The development of adaptive resolution simulation schemes is a subject of growing interest within the community of condensed matter, material science and chemical physics. For adaptive resolution is meant that the space is partitioned in regions characterized by different molecular representation, molecules can freely diffuse among the different regions and change their resolution accordingly. Several approaches have been presented during the last few years, they differ considerably for the level of conceptual rigor and numerical complexity[1–6] (see also ref. 7 for further clarifications). The interest in this kind of approach rises from the fact that in principle it may efficiently tackle the problem of interplay between different scales. This occurs by properly treating, simultaneously, all the relevant molecular degrees of freedom in each region of the simulation box and, because of the free diffusion of molecules from one region to another, properly accounting for density fluctuations. The practical consequences are an optimal employment of computational resources and an efficient analysis of the simulation data. In fact it allows for the reduction of computational costs by treating high resolution models, which are computationally demanding, only in restricted regions, and at the same time assures that details not relevant for the problem are not processed in regions where high resolution is not required. This last aspect allows in turn to derive a clear understanding of the basic physical features characterizing a given problem avoiding an excess of details that can overshadow the essential physics. However while the adaptive idea can be implemented in molecular dynamics codes in a reasonable way, by employing the basic principles of classical dynamics and thermodynamics, when quantum mechanics is considered the situation becomes by far more complicated because it involves not only the change of the number of degrees of freedom, but also the physical principles that govern their evolution. Practical methods[6,8,9] that couple the two regimes in a straightforward way are, in general, not bothered by the "conceptual" discontinuity of passing from a probabilistic (quantum) to a deterministic (classical) approach (and *vice versa*), and base their validity on empirical and numerical criteria only. We have instead developed a scheme where the two regimes are coupled in such a way that the passage from the quantum principles to the classical principles is realized in a smooth, consistent way. The idea consists of considering the atoms described within the path integral formalism, and thus they are represented (effectively) by classical polymer rings (see *e.g.* ref. 10). Within the path integral formalism, a classical polymer ring provides the quantum character of delocalization of an atom, and the interaction site (the center of the sphere in the classical force field) is delocalized on several beads of the polymer. A bead of the polymer is connected to its neighbors by a harmonic spring where the elastic constant depends on the temperature and the number of beads (n) employed, $k = \frac{nm(k_B T)^2}{\hbar^2}$, ($k_B$ Boltzmann constant, $\hbar$ Planck's constant and m the mass of the particle). In this

Max-Planck-Institute for Polymer Research, Ackermannweg 10, D 55021 Mainz, Germany. E-mail: dellsite@mpip-mainz.mpg.de

context the set-up of a consistent framework for adaptive resolution between the quantum (path integral/polymer ring) atom and the classical one corresponds to the coupling of two classical regions with a different number of effective "classical" degrees of freedom. This means that one has polymer rings, each with n classical degrees of freedom, in the quantum region and classical spherical atoms (or coarse-grained molecules as in ref. 11) in the classical region with their associated degrees of freedom. In this way the principles of classical adaptive methods would apply straightforwardly to the quantum-classical case. We have tested this idea for a toy model of a liquid of tetrahedral molecule at standard (ambient) thermodynamic conditions and proved that the basic idea works.[11] The tetrahedral molecules posses enough structural complexity typical of small multiatomic molecules and the study of ref. 11 has been important in proving that a large reduction of the number of degrees of freedom in the adaptive process could be described well by the AdResS method. In fact in the path integral representation of the tetrahedral molecule each atom was represented by 30 beads and thus each molecule has 120 degrees of freedom. The classical coarse-grained representation instead consists of a one site spherical object (3 translational degrees of freedom), thus when a molecule passes from a path integral to a coarse-grained representation the number of degrees of freedom are reduced of a factor 40, and, equivalently, from a coarse-grained to a path integral representation the molecules acquires 117 degrees of freedom. However the toy model does not possess explicit physical properties which naturally ask for a specific quantum treatment of its atoms. For the reason above, in this paper we apply the procedure to a liquid of *para*-hydrogen at low temperatures. Such a system represents a challenging test for the procedure because of: (a) the extreme thermodynamic conditions of low temperature and pressure; and (b) the corresponding strong quantum nature of the hydrogen molecule at these conditions. Moreover, this is a system where the path integral/polymer ring approach is largely employed and thus there exists an extended literature to which one may refer for comparison. In general this test will tell us whether the method can be successfully applied to a molecule of hydrogen in thermodynamic conditions which are by far more challenging that the ambient conditions. If the test is satisfactory then one can be rather confident that the method is robust enough to tackle problems involving hydrogen atoms (*e.g.* as an atomic component of water) at ambient conditions. We show that indeed the method is rather robust and discuss two different algorithms, each with its own convenience given the simulation conditions. It must be also clarified, as it has been already implicitly stated, that here we do not intend to find new results about the liquid *para*-hydrogen, but only reproduce known results in order to validate our approach. The paper is organized as follows; after an overview of the methods used, we then provide the basic physics of a liquid of molecular hydrogen at low temperature and its treatment with path integral. Next we describe the technical aspects of the simulation and finally we discuss the results for the two systems chosen, at the temperature of 25 K and 14 K, and close with the conclusions.

II. Methods

A Path integral molecular dynamics

Let us consider a system of N distinguishable particles described by the Hamiltonian of the form

$$H = \sum_{I=1}^{N} \frac{P_I^2}{2M_I} + V(R_1, \ldots, R_N). \tag{1}$$

The corresponding density matrix in the position space is given by

$$\rho(\mathbf{R},\mathbf{R}';\beta) = \langle \mathbf{R}|e^{-\beta H}|\mathbf{R}'\rangle, \tag{2}$$

with $\beta = 1/k_B T$. The definition of the quantum mechanical partition function is given by the trace of the density matrix:

$$Z \equiv \mathrm{Tr}(e^{-\beta H}) = \int d\mathbf{R}\langle \mathbf{R}|e^{-\beta H}|\mathbf{R}\rangle \tag{3}$$

At this point the Trotter theorem[12] can be used to factorize $e^{-\beta H}$ in a kinetic and a potential part:

$$e^{-\beta(K+V)} = \lim_{n\to\infty}[e^{\frac{-\beta}{2n}V} e^{\frac{-\beta}{n}K} e^{\frac{-\beta}{2n}V}]^n \tag{4}$$

where K is the kinetic and V the potential operator. Substituting the Trotter discretization into eqn (3) and using the definition of the identity operator, $\int|\mathbf{R}\rangle\langle\mathbf{R}|d\mathbf{R}$, $n-1$ times yields:

$$Z = \lim_{n\to\infty}\int d\mathbf{R}^{(1)}\ldots d\mathbf{R}^{(n)}\langle\mathbf{R}^{(1)}|[e^{\frac{-\beta}{2n}V} e^{\frac{-\beta}{n}K} e^{\frac{-\beta}{2n}V}]|\mathbf{R}^{(2)}\rangle\ldots$$

$$\langle\mathbf{R}^{(i)}|[e^{\frac{-\beta}{2n}V} e^{\frac{-\beta}{n}K} e^{\frac{-\beta}{2n}V}]|\mathbf{R}^{(i+1)}\rangle\ldots\langle\mathbf{R}^{(n)}|[e^{\frac{-\beta}{2n}V} e^{\frac{-\beta}{n}K} e^{\frac{-\beta}{2n}V}]|R^{(1)}\rangle. \tag{5}$$

Since the potential is diagonal in $|\mathbf{R}\rangle$, each matrix element takes the form:

$$\begin{aligned}&\langle\mathbf{R}^{(i)}|e^{\frac{-\beta}{2n}V} e^{\frac{-\beta}{n}K} e^{\frac{-\beta}{2n}V}|\mathbf{R}^{(i+1)}\rangle \\ &= e^{\frac{-\beta}{2n}V(\mathbf{R}^{(i)})}\langle\mathbf{R}^{(i)}|e^{\frac{-\beta}{n}K}|\mathbf{R}^{(i+1)}\rangle e^{\frac{-\beta}{2n}V(\mathbf{R}^{(i+1)})}.\end{aligned} \tag{6}$$

At this point using the identity operator in momentum space, $\int|\mathbf{P}\rangle\langle\mathbf{P}|d\mathbf{P}$, the remaining matrix elements can be written as:

$$\begin{aligned}\langle\mathbf{R}^{(i)}|e^{\frac{-\beta}{n}K}|\mathbf{R}^{(i+1)}\rangle &= \int d\mathbf{P}\langle\mathbf{R}^{(i)}|\mathbf{P}\rangle\langle\mathbf{P}|e^{\frac{-\beta}{n}K}|\mathbf{R}^{(i+1)}\rangle \\ &= \int d\mathbf{P}\langle\mathbf{R}^{(i)}|\mathbf{P}\rangle\langle\mathbf{P}|\mathbf{R}^{(i+1)}\rangle e^{-\beta P^2/(2Mn)}\end{aligned} \tag{7}$$

which can be simplified further by using the projection of a momentum eigenstate on a position eigenstate

$$\langle\mathbf{R}|\mathbf{P}\rangle = \frac{1}{\sqrt{2\pi\hbar}} e^{i\mathbf{P}\cdot\mathbf{R}/\hbar}. \tag{8}$$

In fact replacing eqn (8) into eqn (7) one gets:

$$\langle\mathbf{R}^{(i)}|e^{\frac{-\beta}{n}K}|\mathbf{R}^{(i+1)}\rangle = \left(\frac{Mn}{2\pi\beta\hbar^2}\right)^{1/2} e^{-\frac{Mn}{2n\beta\hbar^2}(\mathbf{R}^{(i)}-\mathbf{R}^{(i+1)})^2}. \tag{9}$$

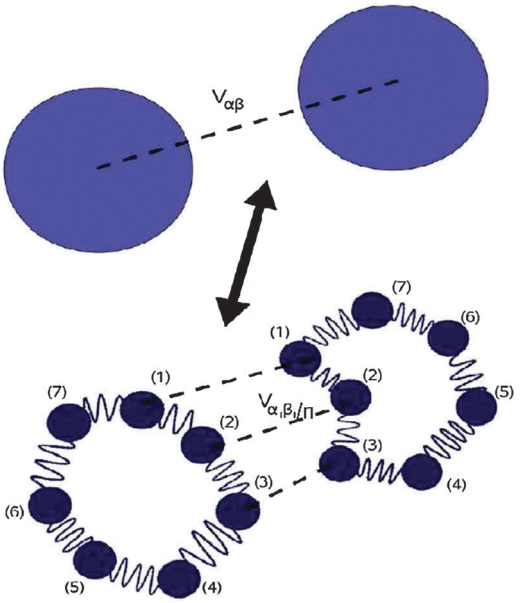

Fig. 1 Path integral representation of two quantum particles for $n = 7$ beads (Trotter number).

Substituting this last results into the eqn (5) one obtains:

$$Z = \lim_{n\to\infty}\left[\prod_{I=1}^{N}\left(\frac{Mn}{2\pi\beta\hbar^2}\right)^{n/2}\int d\mathbf{R}_I^{(1)}\ldots d\mathbf{R}_I^{(n)}\right] \times e^{-\beta\sum_{I=1}^{N}\sum_{s=1}^{n}\frac{1}{2}M_I\omega_n^2(R_I^{(s)}-R_I^{(s+1)})^2+\frac{1}{n}V(\{R_I^{(s)}\})}, \quad (10)$$

where the effective path integral Hamiltonian is given by

$$\mathscr{H}_n = \sum_{I=1}^{N}\sum_{s=1}^{n}\frac{1}{2}M_I\omega_n^2(R_I^{(s)}-R_I^{(s+1)})^2+\frac{1}{n}V(\{R_I^{(s)}\}). \quad (11)$$

Eqn (11) is formally equivalent to the classical interactions of N ring-polymers consisting of n beads each connected by harmonic springs and with a polymer–polymer interaction as sketched in Fig. 1. Note that the bead–bead interaction between different polymers is attenuated by a factor $1/n$. Here $\omega_n = m\sqrt{n}(k_BT)/\hbar$ is the frequency of the ring-polymer, n is the Trotter number, T the temperature and M is the physical mass. The calculation of Z in eqn (11) requires a sampling of the configurational space of the N ring-polymers; in order to devise a molecular dynamics scheme to calculate Z, one has to add n-Gaussian integrals in the momentum space to eqn (10) and this gives,

$$Z = \lim_{n\to\infty}\left[\prod_{I=1}^{W} W\int d\mathbf{R}_I^{(1)}\ldots d\mathbf{R}_I^{(n)}\int d\mathbf{P}_I^{(1)}\ldots d\mathbf{P}_I^{(n)}\right] \times e^{-\beta\sum_{I=1}^{N}\sum_{s=1}^{n}\frac{[P_I^{(s)}]^2}{2M_I'}+\frac{1}{2}M_I\omega_n^2(R_I^{(s)}-R_I^{(s+1)})^2+\frac{1}{n}V(\{R_I^{(s)}\})}, \quad (12)$$

where W is a proper normalization factor and M_I' is the fictitious mass of the beads. The momenta $\mathbf{P}_I$ are fictitious quantities that allow mapping of the static problem of the interacting ring-polymers into a dynamical sampling, however they do not have any physical meaning. The Hamiltonian for the molecular dynamics scheme can now be written explicitly as:

$$\mathscr{H}_n(\mathbf{R},\mathbf{P}) = \sum_{I=1}^{N}\sum_{s=1}^{n}\frac{[P_I^{(s)}]^2}{2M_I'}+\frac{1}{2}M_I\omega_n^2(R_I^{(s)}-R_I^{(s+1)})^2+\frac{1}{n}V(\{R_I^{(s)}\}) \quad (13)$$

The approach illustrated above is commonly known as the path integral molecular dynamics (PIMD) in the real space. Within PIMD the ring–polymer dynamics can be employed to evaluate the expectation value of any observable A as follows:

$$\langle A\rangle = \lim_{n\to\infty}\left[\prod_{I=1}^{N} W\int d\mathbf{R}_I^{(1)}\ldots d\mathbf{R}_I^{(n)}\int d\mathbf{P}_I^{(1)}\ldots d\mathbf{P}_I^{(n)}\right] \times e^{-\beta\mathscr{H}_n(\mathbf{R},\mathbf{P})}A_n(\mathbf{R}) \quad (14)$$

where A_n is calculated over the ring–polymer trajectories:

$$A_n(\mathbf{R}) = \frac{1}{n}\sum_{s=1}^{n}A(\mathbf{R}_1^{(s)},\ldots,\mathbf{R}_N^{(s)}) \quad (15)$$

B The adaptive resolution simulation scheme (AdResS)

The basic requirement of an adaptive resolution method is that the change of resolution occurs without perturbing the thermodynamic equilibrium;[13–19] this is done by the extensively tested AdResS method,[20–23] within a Molecular Dynamics scheme, which we employ in this work. In the AdResS method the molecular resolution is changed on-the-fly during a simulation as a molecule transits from the a high resolution region (*e.g.* atomistic) to a low resolution region (*e.g.* coarse-grained). The exchange of the molecules between the different regions occurs under condition of thermodynamic equilibrium, that is: $\rho_{atom} = \rho_{cg}$ (density equilibrium); $P_{atom} = P_{cg}$ (pressure equilibrium); $T_{atom} = T_{cg}$ (thermal equilibrium). The thermodynamic state point is the same as that of a full atomistic system. From the technical point of view the method consists of a two step procedure: (a) derive an effective (coarse-grained) potential from the reference atomistic simulation; (b) couple the two regimes *via* a space dependent interpolation formula on the forces (see *e.g.* ref. 1 and 24):

$$\mathbf{F}_{\alpha\beta} = w(X_\alpha)w(X_\beta)\mathbf{F}_{\alpha\beta}^{atom} + [1 - w(X_\alpha)w(X_\beta)]\mathbf{F}_{\alpha\beta}^{cg} \quad (16)$$

α and β are the two molecules, $\mathbf{F}^{atom}$ is the atomistic force and $\mathbf{F}^{cg}$ is the coarse-grained one, X is the x coordinate of the molecular center of mass and w is a "switching" function which smoothly interpolates the forces. w is 0 in the coarse-grained/lower resolution region and 1 in the atomistic/high resolution region, while it is continuous and monotonic in between (hybrid/transition region), as illustrated in Fig. 4. This procedure assures that when a molecule passes from a region with atomistic resolution to a region with coarse-grained resolution the switching function w smoothly "freezes" the dynamical evolution of those degrees of freedom that are switching off (that is those that the molecule is losing) and their contribution to the interactions with the rest of the system. *Vice versa*, when a molecule follows the opposite path (coarse-grained to atomistic), w smoothly reactivates the dynamics of the switching degrees of freedom (that the molecule is now acquiring) and their contribution to the

interactions with the rest of the system. By construction the third Newton's Law is conserved, a crucial point for a molecular dynamics scheme. Essentially what eqn (16) does is to allow for a smooth transition from an atomistic to a coarse-grained (and *vice versa*) dynamics keeping the perturbation due to the change of resolution as small as possible. However eqn (16) implies a non-Hamiltonian approach and the lack of a conserved energy poses the question of how one can assure the control of the thermodynamic equilibrium of the system, as this latter is an essential ingredient for a conceptually correct adaptive scheme. We have shown that a scheme based only on eqn (16) would create a "resolution dependent" chemical potential across the simulation box. This implies a preferential tendency of the molecules to migrate towards the region of lower chemical potential which in turn leads to an unphysical inhomogeneous density across the box.[1] This problem is solved by interpreting the resolution dependent chemical potential in terms of some "latent heat" acquired by the molecule (acquiring degrees of freedom, *e.g.* vibrational and rotational) or released by the molecule (losing degrees of freedom). We have shown that this process of acquiring or releasing heat can be properly taken into account by a locally acting thermostat.[1] In order to reach high accuracy a thermodynamic force which balances the chemical potential across the box can be added.[2] However, in most of the cases (as the one treated in this work), the thermostat is sufficient to assure that the discrepancy between the results of the adaptive simulation and those of a full atomistic simulation stays within a 5% difference. Moreover, it has been shown that the use of the forces rather than the potentials is conceptually more rigorous[15–17] (see also ref. 7 for further explanations). The effective coarse-grained potential, at a given thermodynamic conditions, is derived from a reference all-atom simulation employing (typically) an iterative inverse Boltzmann procedure that matches the molecular center of mass radial distribution.[25] In the case of the quantum-classical adaptive scheme, the same procedure as for the classical case applies. The difference is that the atoms are described as polymer rings in a path integral approach and the effective coarse-grained potential for a molecule is derived from a full path integral reference simulation at the given thermodynamic state point. This means that the interpolation according to w occurs between $\mathbf{F}^{\mathrm{pi}}$ acting on the beads of the rings (which now plays the equivalent role of $\mathbf{F}^{\mathrm{atom}}$ in eqn (16)) and the $\mathbf{F}^{\mathrm{cg}}$ derived from the effective coarse-grained potential acting among the centers of mass of the molecules (of both path integral and coarse grained representation).

III. Liquid of molecular hydrogen: basic physics

The liquid and solid phases of molecular hydrogen and deuterium have been extensively studied experimentally[26] and theoretically.[27,28] These many-body systems continue to appear in very fundamental problems for several reasons. It is known that hydrogen molecules are the principal constituent of distant planets[29] and in the field of high-pressure physics the hydrogen exhibits the fluid metal–insulator transition.[30,31] The spectrum of molecular hydrogen in the liquid phase exhibits the effect of the internal nuclear degrees of freedom which leads to the characterization of two spin isomers of hydrogen diatomic molecules and different levels of excitations. One of the isomeric forms is the *ortho*-hydrogen where its two proton spins are aligned parallel and form a triplet with a total spin quantum number of $J = 1$; in the other form, the *para*-hydrogen, its proton spins are aligned antiparallel and form a singlet with a total spin quantum number of $J = 0$.

A The path integral description of *para*-hydrogen

In general, liquid hydrogen does not exhibit the strong identical particle exchange effects typically observed in liquid helium, and thus the physics of the system is simplified. In fact even at very low temperature (*e.g.* around the triple point, 13.8 K) the thermal de Broglie wavelength $\lambda = h/(2\pi m k_{\mathrm{B}} T)^{1/2} = 3.3$ Å, is slightly larger than the mean distance between two hard spheres in the classical representation of hydrogen in a molecules ($\sigma = 3.0$ Å). This implies that the exchange of identical *para*-hydrogen molecules will not have a pronounced effect in the properties of the liquid phase[32,33] and therefore the *para*-hydrogen molecules follow the Boltzmann statistics. Another characteristic of the liquid molecular hydrogen at low temperatures is the inversion of the predominant population, *i.e.* *ortho*-hydrogen at room temperature to the *para*-hydrogen at lower temperatures. Since the majority of the *para*-hydrogen molecules are in the ground state ($J = 0$) , the wave functions that characterize such a molecular state are spherically symmetric; this means that the interaction between molecules can be modeled by an effective isotropic pair potential[34] (see Fig. 2). Details of the classical potential are provided in the Technical section. Due to the inherent quantum behavior of the *para*-hydrogen molecules at low temperatures, several computational techniques based on the path integral formulation of quantum mechanics became routine methods to calculate static (*e.g.* ref. 35 and 36) and dynamic (*e.g.* ref. 37–40) properties of this quantum liquid. In Fig. 2 we show the conceptual transition from the (effective spherical) classical model to the corresponding quantum (polymer ring) model by means of the path integral approach.

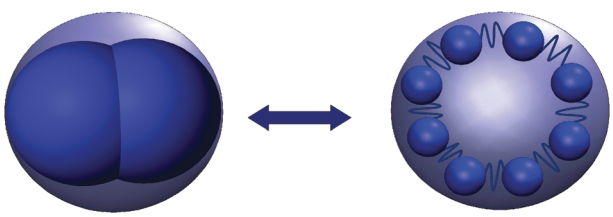

Fig. 2 Quantum representation of the *para*-hydrogen by the path integral approach. On the left side the classical form for a diatomic hydrogen molecule is depicted where the shadowed sphere indicates that the classical intermolecular potential is isotropic. On the right side is depicted the corresponding quantum description of the molecule by a ring–polymer representation within the path integral approach. In this latter case the interaction between polymer a and polymer b occurs only between pairs of beads with the same index i, *i.e.* $\mathrm{a}_i\mathrm{b}_i$.

IV. *para*-Hydrogen in AdResS

In Fig. 3 we illustrate the transition of the molecule from a classical one site coarse grained representation to a quantum representation by means of the path integral approach, in between is depicted the hybrid representation. The adaptive method AdResS applies as in the classical case. First we perform a full path integral/polymer ring simulation of the liquid system, taking the structural properties of such a system (center of mass radial distribution function, RDF) as a reference. Next we derive an effective potential acting on the center of the ring and use this as a coarse-grained model for a (spherical) classical representation of the *para*-hydrogen molecule in the adaptive simulation. This step of the procedure provides structural consistency between the two representations used.[41] Next the adaptive resolution molecular dynamic simulation is performed according to the AdResS algorithm as it is schematically depicted in Fig. 4.

A Technical details of the simulation

To perform path integral simulations we have used the isotropic part of the Silvera–Goldman pair potential,[34] standard in several study employing this approach for *para*-hydrogen liquid at the given thermodynamic conditions specified below.

$$V(r) = e^{\alpha-\beta r-\gamma r^2} - \left(\frac{C_6}{r^6}+\frac{C_8}{r^8}+\frac{C_{10}}{r^{10}}\right)f_c(r)+\frac{C_9}{r^9}f_c(r), \quad (17)$$

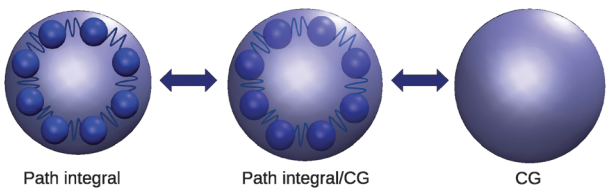

Fig. 3 Adaptive resolution scheme for *para*-hydrogen; the high resolution on the left corresponds to the quantum path integral representation. The low resolution on right corresponds to the effective spherical classical model obtained by coarse-graining the high resolution representation. This latter is obtained by iterative inverse Boltzmann procedure which reproduces structural properties of full path integral reference simulations of the liquid. In the middle the hybrid resolution as the molecules is continuously transformed from a quantum to a classical representation.

Table 1 Parameters used in the Silvera–Goldman pair potential (in atomic units)

α	1.713	C_6	12.14
β	1.5671	C_8	215.2
γ	0.00993	C_9	143.1
r_c	8.32	C_{10}	4813.9

where

$$f_c(r) = \begin{cases} e^{-(r_c/r-1)^2}, & \text{if } r \le r_c \\ 1, & \text{otherwise,} \end{cases} \quad (18)$$

The first term on the right-hand side in eqn (17) corresponds to the short-range repulsive interaction, while the second term describes the long-range attractive interaction. The last term, C_9/r^9, is an effective two body approximation to the three-body dispersion interaction. The $f_c(r)$ is used to screen the effect of the attractive interaction at short distance. The value of the parameters are listed in Table 1. $V(r)$ is shown in Fig. 5.

In our simulations we consider two cases at two different temperature (14 K and 25 K respectively) and use the theoretical number density obtained from the earlier path integral Monte Carlo (PIMC)[32] calculations (ρ = 0.0035 (bohr)$^{-3}$ at 14 K and ρ = 0.0028 (bohr)$^{-3}$ at 25 K), at zero pressure. Atomic units (*i.e.* $e,\hbar,m$ = 1) are used and this means that the unit of energy is given in Hartree (E_h = 4.3597 × 10^{-18} J) and the distance in atomic bohr (a_0 = 0.529 Å). The interaction between bead–bead of neighboring ring-polymers was truncated at

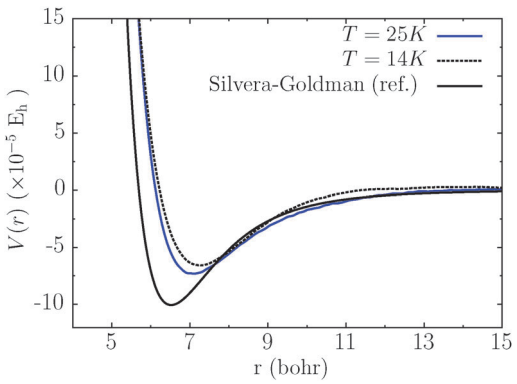

Fig. 5 A plot of the potentials resulting from the Iterative Boltzmann Inversion (IBI) procedure. The solid (blue) line corresponds to T = 25 K, ρ = 0.0028 (bohr)$^{-3}$ and the (black) dashed line for T = 14 K, ρ = 0.0035 (bohr)$^{-3}$. The classical Silvera and Goldman potential[34] in solid (black) line is also depicted.

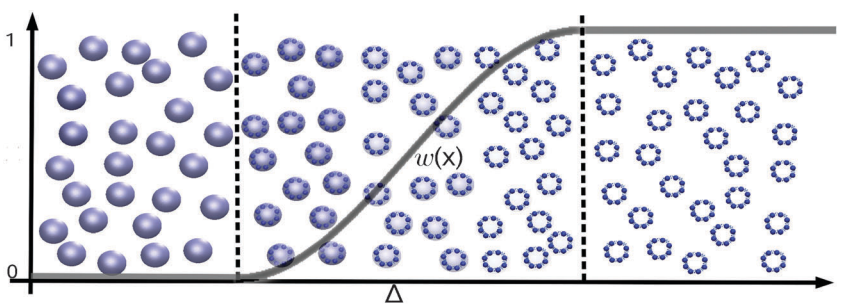

Fig. 4 AdResS set up for the *para*-hydrogen liquid.

15 bohr. From the earlier simulation with PIMC it is known that for the low temperature case (T = 14 K) the quantum character of *para*-hydrogen becomes stronger and the number of beads used in the path integral approach should be increased to 48. For the higher temperature (T = 25 K) case, 28 beads are enough to guarantee the convergence of the static properties. We perform simulations employing two different approaches to path integral: (a) path integral formulation in the primitive space PIMD (real space) which is computationally less demanding but proves not to be accurate enough for the lower temperature; and (b) the path integral formulation in terms of normal modes (PIMD + NM), computationally more-demanding but more accurate at the lower temperature. In fact at the lower temperature the use of a larger number of beads leads to the situation that the bead–bead interaction between corresponding beads of different polymer becomes less relevant due to the fact that (as it follows from the path integral formalism) it scales as $\frac{1}{n}V_{a_i,b_i}$ (a_i indicates the ith bead of the polymer representing molecule a, same for b). At the same time the bead–bead interaction between bonded neighboring beads of the same polymer becomes dominant because it scale as n. In this situation problems of ergodicity arise in a real space approach, instead the normal mode approach, by ensuring the proper sampling of all the frequency of the system, solves the problem.[43] In practice this method allows for propagating all the modes over the same time step and thus the time scale of the integration is non pathological (see also the section VIII). Each simulation discussed here was equilibrated for 100 ps and then the static properties were calculated by averaging over 1000 consecutive 10 ps path integral trajectories with a time step equal to 0.5 fs.

B Effective coarse grained potential

To obtain an effective one-site coarse grained (CG) potential from the path integral representation of *para*-hydrogen we used the standard procedure known as the Iterative Boltzmann Inversion (IBI).[25] Such a procedure derives an effective potential given the center-of-mass RDF as a target from the full explicit path integral simulation. Although the pressure must be zero for both thermodynamic state points, a pressure correction has been performed as it is routinely required to get as close as possible to the target pressure (see for example ref. 44). In this aspect the coarse-graining procedure at these thermodynamic conditions becomes more difficult since the large pressure fluctuations (of the order of 10^{-7} E_h/bohr^{-3}) and the inherent error of the iterative procedure lead to a large relative error on the pressure of the coarse-grained model. For each system the IBI was applied over 30 iterations until convergence of the target radial distribution was reached. Each iteration consists of 50 ps and 500 ps of equilibration and production respectively. Our results are shown in Fig. 5 where we plot the effective CG potential obtained for each temperature studied and for comparison is depicted the classical Silvera and Goldman potential. As one can see the effective potential becomes less attractive and the minima of the potential is shifted as the temperature decreases from T = 25 K to T = 14 K.

V. Results

In this section we present the result of our approach in AdResS for the two thermodynamic state points studied. The path integral implementation in the real space will be denoted by PIMD and the Normal Modes implementation as PIMD + NM.

A For T = 25 K

This thermodynamic state represents a "less quantum" system with Trotter number (number of beads) n = 28 compared to the other system at T = 14 K shown later. As one can see in the Fig. 6(a) for the bead–bead RDF in the full (explicit) path integral simulation the PIMD and PIMD + NM implementation perform quite well and no differences are found compared to the reference data.[32] In part (b) and (c) we report the

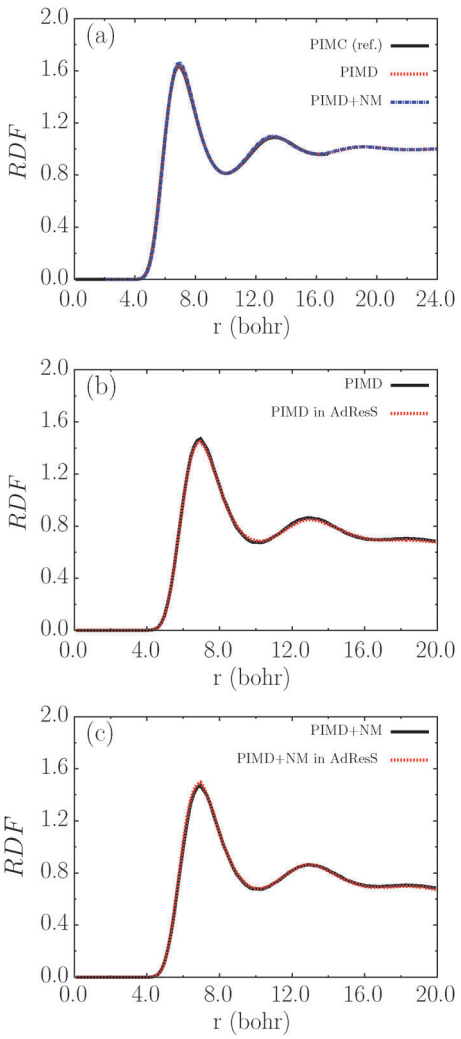

Fig. 6 (a) Comparison of the bead–bead RDF in a full explicit path integral simulation at T = 25 K. The PIMD and PIMD + NM are compared to earlier work[32] (whose data are available up to 16 bohr) and full agreement is obtained. (b) The bead–bead partial RDF calculate only in the region corresponding to the quantum region in AdResS for the PIMD compared with the same quantity calculated in the PIMD/AdResS approach. (c) Shows the same as in (b), but for the PIMD + NM implementation.

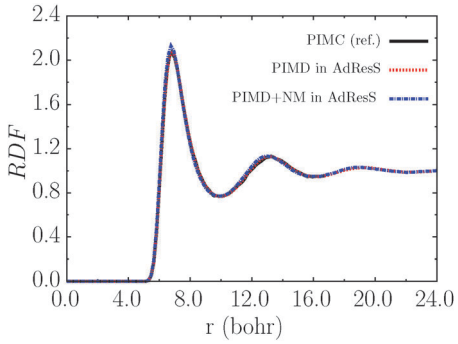

Fig. 7 Center-of-mass RDF evaluated in the whole box at $T = 25$ K. The agreement between the ref. 32 calculation, the PIMD in AdResS and PIMD + NM in AdResS are highly satisfactory.

bead–bead RDF obtained within AdResS, with PIMD and the PIMD + NM, calculated in the quantum region of the adaptive resolution system. This is here compared with the RDF calculated in the same subregion but from a full explicit path integral simulation. The agreement is highly satisfactory. In Fig. 7 we compare the center-of-mass RDF in all the box for the PIMD and PIMD + NM in AdResS and compare it with the reference data; also in this case a full agreement is found at this temperature. To complete the prove that in the adaptive simulation a valid thermodynamic equilibrium is reached we calculate the density profile in Fig. 8. This shows the typical 5% drop of density in the hybrid region (Δ) which is compensated by the increment of the density in the path integral and coarse grained regions.[11] The slightly larger density in the coarse-grained region is mostly due to the above-mentioned problem of the difficulties of targeting the coarse-grained model to the exact pressure of the high resolution system. However the agreement is rather satisfactory. Finally in order to check the free diffusion and exchange of particles across the regions we calculated the diffusion profile in Fig. 9; this proves that indeed the molecules move through the hybrid region diffusing from the high resolution to the low resolution and *vice versa*.

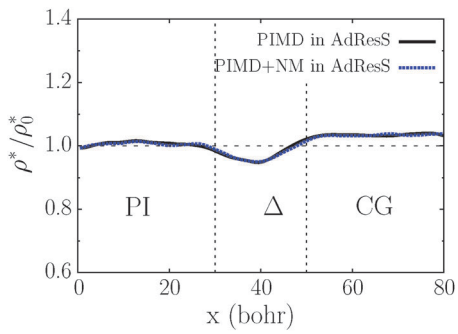

Fig. 8 Normalized density profile along the x direction at $T = 25$ K in AdResS. The vertical lines denote the boundaries between the path integral (PI), coarse grained (CG) and hybrid (△) regions of the system. In the Figure is depicted the case of both PIMD and PIMD + NM within the AdResS scheme. The drop of density in the hybrid region is about 5% of the reference value (horizontal dashed line), while the overestimation in the CG region compared to that in the PI region is below 2%.

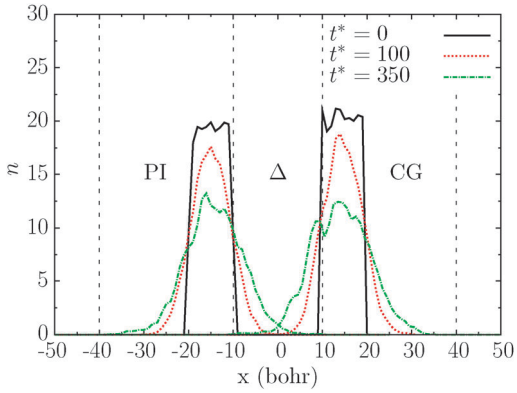

Fig. 9 Diffusion profile for *para*-hydrogen molecules from the CG to the PI region and *vice versa*. Here showed for the case of PIMD (a similar profile was obtained also for the PIMD + NM case, for simplicity not reported here).

B For $T = 14$ K

This case represents a "more quantum" situation due to the larger Trotter number used, $n = 48$. As one can see in the Fig. 10(a) the path integral implementation in the real space (PIMD) does not converge to the reference data and only its implementation with the normal modes reproduces the reference structure of the system[32] in a full explicit simulation. This means that PIMD in AdResS will also not reproduce the true physics of the system, and for this reason we will not consider it here. This is instead the case where the PIMD + NM becomes ideal and for this reason we test his performance in the adaptive scheme. Fig. 10(b) shows the comparison between the partial bead–bead RDF (calculated as in Fig. 6) for the full explicit PIMD + NM and that of the PIMD + NM in AdResS; a rather satisfactory agreement is found. In part (c) the center-of-mass RDF for the PIMD + NM in AdResS with the reference data[32] is compared and satisfactory agreement is found. Similarly to the previous case we show the density profile in Fig. 11 for the PIMD + NM and once again we note a satisfactory agreement. The same can be said for the diffusion profile shown in Fig. 12.

VI. Discussion and conclusions

We have reported an application of the AdResS classical/path-integral method, to the liquid of *para*-hydrogen at two different temperatures, namely 25 K and 14 K. These two systems represent a challenging test for the method because of the dominant character of the quantum effects. We have presented two different algorithms, one based on the real space treatment of the polymer rings representing the atoms, and one on the normal mode treatment of them. The first is computationally less demanding but loses precision as the number of beads in the polymer increases, the second is computationally more demanding but can well describe situations where the number of beads is large. In any case, for both approaches we have shown that the adaptive method AdResS reproduces in a rather satisfactory way the static properties of the liquid when compared to the results of full explicit path integral simulations and to those available in

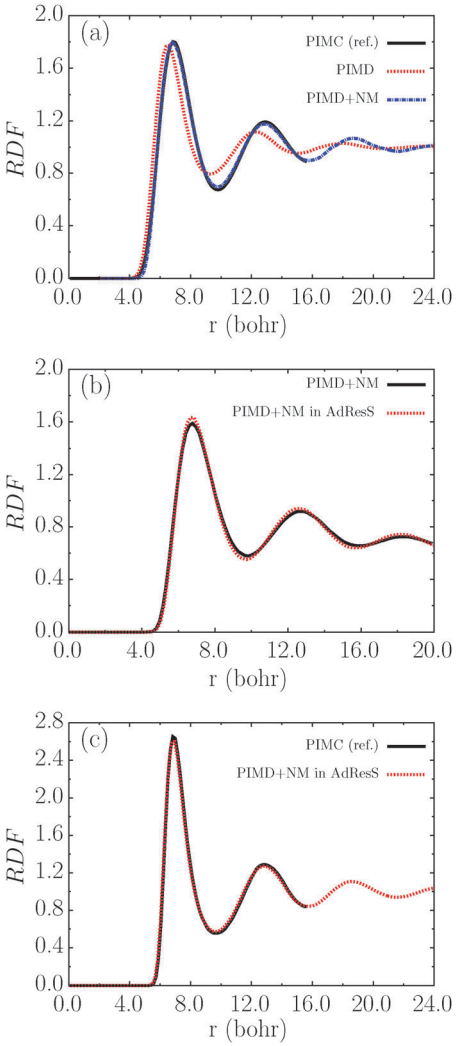

Fig. 10 (a) Comparison of the bead–bead RDF in a full explicit path integral simulation at $T = 14$ K. PIMD and PIMD + NM are compared to earlier work.[32] Agreement between the reference data and PIMD + NM is obtained while PIMD shows to not be appropriate at this temperature. (b) Bead–bead partial RDF for a full explicit PIMD + NM and in AdResS. (c) Center-of-mass RDF for PIMD + NM in AdResS compared to the reference data (available up to 16 bohr).

literature. The message of this work is that since at ambient conditions the quantum effects can be important, but not dominant, and the coarse-graining procedure is technically simpler, the adaptive classical/path integral method can be applied with confidence to standard systems in soft matter, chemical physics and condensed matter. For example one may think of extending the classical AdResS study of the locality of hydrogen bond network at hydrophobic surfaces[23] to the case where the quantum nature of the protons of water is considered. The application of this scheme would tell us whether the conclusions reached with classical models hold in the presence of quantum effects. This is only one representative example where the method can be applied and in this context this work has shown that there are no conceptual or technical barriers to proceed along these directions in applications.

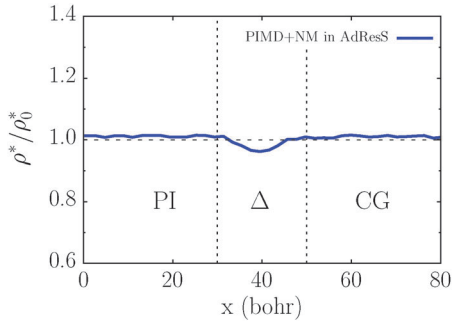

Fig. 11 As in Fig. 8 but for $T = 14$ K and only in the case of PIMD + NM. The more symmetric distribution between the PI and CG region compared to Fig. 8 is not due to some systematic improvements but to a mere numerical coincidence. In general one expects for thermodynamic state points similar to those treated here that the results of Fig. 8 are more common that those in the figure above. This, as underlined in several points of this paper, is mainly due to the numerical difficulty of targeting the (almost zero) pressure and to the corresponding large relative error.

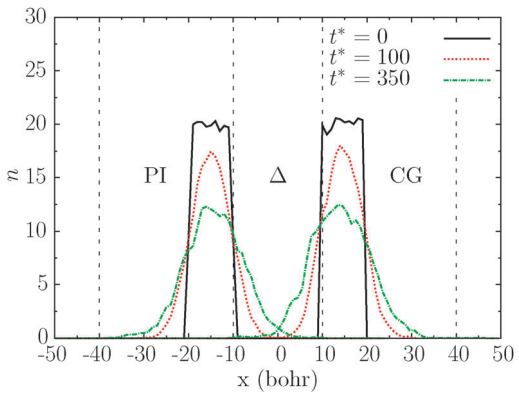

Fig. 12 As in Fig. 9 but at temperature $T = 14$ K and only for the PIMD + NM case.

VII. Appendix: Implementation of the normal modes (NM) in AdResS

The Hamiltonian in the path integral approach for N particles interacting by the force field $V(R)$ is given by eqn (13). The direct use in molecular dynamics of such a scheme becomes inefficient as the number of beads n becomes large. In fact as this number increases, the harmonic spring terms become stiffer and the neighboring bead–bead intra-polymer interaction dominates the dynamics over the inter-polymer bead–bead interaction which is instead scaled by $\frac{1}{n}$. In this situation the sampling of the frequencies is not properly done. A solution for this problem is given by normal mode transformation which allows to carry out the evolution of all the frequencies (see ref. 10 and also ref. 45). For a large n the harmonic modes have to be decoupled so that one can move all the modes over the same simulation time scale. In order to do so the harmonic potential from eqn (13) is expressed as a sum of n uncoupled harmonic oscillators. This, in vector notation, writes as:

$$V_I(\{R_I^{(s)}\}) = \tfrac{1}{2} M_I \omega_n^2 \mathbf{R}_I^T \cdot \mathbf{A} \cdot \mathbf{R}_I \qquad (19)$$

where **A** is the matrix that couples the coordinates of different beads. One can transform **A** in a decoupled form by diagonalization. This is done analytically by expressing eqn (19) in the normal modes variables as follows:

$$V_I(\{Q_I^{(s)}\}) = \tfrac{1}{2}M_I\omega_n^2\mathbf{Q}_I^T\cdot\mathbf{a}\cdot\mathbf{Q}_I \qquad (20)$$

where **a** is a diagonal matrix and $\mathbf{Q}_I$ are the normal modes. Now using the property of **a** being diagonal, the eqn (19) become

$$V_I(\{Q_I^{(s)}\}) = \frac{1}{2}M_I\omega_n^2\sum_{s=1}^{n}a_sQ_s^2 = \sum_{s=1}^{n}\frac{1}{2}M_I\Omega_s^2Q_s^2 \qquad (21)$$

which has the form of n uncoupled harmonic oscillators with normal-modes frequencies equal to:

$$\Omega_s = \omega_n\sqrt{a_s} = 2\omega_n\sin(s\pi/n). \qquad (22)$$

We use the Hamiltonian from eqn (13) in the Normal Modes variables without external potential to derive the equation of motion (EOM) of a free ring polymer. In the new system of coordinates the EOM takes the form:

$$P_I^{(s)} = \frac{\mathrm{d}Q_I^{(s)}}{\mathrm{d}t}$$

$$\frac{\mathrm{d}}{\mathrm{d}t}P_I^{(s)} = -M_I\Omega_s^2Q_I^{(s)}, \quad \forall s = 1,\ldots,n, \qquad (23)$$

These are the EOM of a n-decoupled harmonic oscillators and the solution is known to be at time $t + \Delta t$:

$$Q_I^{(s)}(t+\Delta t) = Q_I^{(s)}(t)\cos(\Omega_s\Delta t) + \frac{P_I^{(s)}(t)}{M_I\Omega_s}\sin(\Omega_s\Delta t)$$

$$P_I^{(s)}(t+\Delta t) = -Q_I^{(s)}(t)\Omega_sM_I\sin(\Omega_s\Delta t) + P_I^{(s)}(t)\cos(\Omega_s\Delta t) \qquad (24)$$

for all $s = 1,\ldots,n$ and where $Q_I^{(s)}(t)$ and $P_I^{(s)}(t)$ are the initial conditions at time t. In a matrix form,

$$\begin{bmatrix} P_I^{(s)}(t+\Delta t) \\ Q_I^{(s)}(t+\Delta t) \end{bmatrix} = \begin{pmatrix} \cos(\Omega_s\Delta t) & -\Omega_sM_I\sin(\Omega_s\Delta t) \\ \frac{\sin(\Omega_s\Delta t)}{\Omega_sM_I} & \cos(\Omega_s\Delta t) \end{pmatrix} \begin{bmatrix} P_I^{(s)}(t) \\ Q_I^{(s)}(t) \end{bmatrix}$$

For simplicity we show the component of the matrices for the zero-frequency (*i.e.* for the centroid), this is the case of $s = 0$ and from the previous matrix we get

$$\begin{bmatrix} P_I^{(0)}(t+\Delta t) \\ Q_I^{(0)}(t+\Delta t) \end{bmatrix} = \begin{pmatrix} 1 & 0 \\ \Delta t/M_I & 1 \end{pmatrix} \begin{bmatrix} P_I^{(0)}(t) \\ Q_I^{(0)}(t) \end{bmatrix}$$

where we used the property of $\lim_{x\to 0}\frac{\sin(x)}{x} = 1$. This form is ideal for the numerical implementation of the algorithm. Now let us synthesize the changes in the velocity Verlet algorithm to perform the NM in few steps:

STEPs of Velocity Verlet with NM in AdResS:

(1) Calculate forces using AdResS. Evaluate $F_I^{(s)}(t)$ only from the external potential contribution in the primitive space.

(2) Update velocities, $v_I^{(s)}(t+\frac{\Delta t}{2}) = v_I^{(s)}(t) + \frac{\Delta t}{2}F_I^{(s)}(t)$, in the primitive space.

(3) Evolve positions and velocities at $t + \Delta t$ with **NM algorithm** (see below).

(4) Calculate forces, $F_I^{(s)}(t+\frac{\Delta t}{2})$ as in STEP 1 from positions of STEP 3.

5. Update velocities, $v_I^{(s)}(t+\Delta t) = v_I^{(s)}(t+\frac{\Delta t}{2}) + \frac{\Delta t}{2}F_I^{(s)}(t+\Delta t)$, in the primitive space.

The STEP 3 concerns the implementation of the Normal Modes and it is presented below

NM algorithm:

(1) Apply the forward FFT to $\{r_I^{(s)}(t)\}$, $\{p_I^{(s)}(t)\} \rightarrow \{Q_I^{(s)}(t)\}$, $\{P_I^{(s)}(t)\}$ (coordinates and momenta in NM).

(2) Evolve $\{Q_I^{(s)}(t)\}$, $\{P_I^{(s)}(t)\}$ according EOM of free ring-polymer (eqn (24)) to $t + \Delta t$.

(3) Apply the backward FFT to $\{Q_I^{(s)}(t + \Delta t)\}$, $\{P_I^{(s)}(t + \Delta t)\} \rightarrow \{r_I^{(s)}(t + \Delta t)\}$, $\{p_I^{(s)}(t + \Delta t)\}$.

Acknowledgements

ABP acknowledge the financial support of the German Academic Exchange Service (DAAD), LDS that of the MMM initiative of the Max-Planck Society. The authors thank S. Fritsch, R. Potestio, C. Junghans and K. Kremer for a critical reading of the manuscript. We also thank D. Manolopoulos for a critical reading of the manuscript and for the precious help, from him and his group, at the initial stage of this project.

References

1 M. Praprotnik, L. Delle Site and K. Kremer, *Annu. Rev. Phys. Chem.*, 2008, **59**, 545.
2 S. Poblete, M. Praprotnik, K. Kremer and L. Delle Site, *J. Chem. Phys.*, 2010, **132**, 114101.
3 B. Ensing, S. O. Nielsen, P. B. Moore, M. L. Klein and M. Parrinello, *J. Chem. Theory Comput.*, 2007, **3**, 1100; S. O. Nielsen, R. E. Bulo, P. B. Moore and B. Ensing, *Phys. Chem. Chem. Phys.*, 2010, **12**, 12401.
4 A. Heyden and D. G. Truhlar, *J. Chem. Theory Comput.*, 2008, **4**, 217.
5 S. Izvekov and G. A. Voth, *J. Chem. Theory Comput.*, 2009, **5**, 3232.
6 M. G. Guthrie, A. D. Daigle and M. R. Salazar, *J. Chem. Theory Comput.*, 2010, **6**, 18.
7 In ref. 17 it has been shown that if the two resolutions are coupled through the interpolation of forces as the one used in AdResS, then it cannot exist as a Hamiltonian from which the interpolated forces can be derived and a standard energy conserved. In ref. 3 and 9 has been instead argued that in a scheme as AdResS the energy can be conserved, however they do not provide an explicit Hamiltonian and state that the potential would depend on the path the molecules follow.[9] The major advantage of having an explicit Hamiltonian in an adaptive scheme consists of the fact that one would have a well defined statistical ensemble and could explicitly write the Boltzmann-like factor, thus control deterministically the delicate issue of the thermodynamic equilibrium of a mixed resolution. In this context, to state that the energy can be conserved but a Hamiltonian cannot be written would in any case be not useful. Moreover the conclusions of ref. 3 and 9 reported above are somehow confusing because by the very definition of a conservative system, a potential must depend only on the positions. Further a potential that depends on the paths of the molecules would be "configuration" dependent, that is it would carry entropic contributions and thus rather than a potential energy it would be a free energy type of term. In fact, in AdResS we have already considered and properly described this situation with the introduction of the concept of latent heat first[15,16] and thermodynamic force later.[2] Such concepts were derived from first principles of thermodynamics and statistical mechanics.
8 A. Heyden, H. Lin and D. G. Truhlar, *J. Phys. Chem. B*, 2007, **111**, 2231.

9 R. Bulo, B. Ensing, J. Sikkema and L. Visscher, *J. Chem. Theory Comput.*, 2009, **5**, 2212.
10 M. E. Tuckerman, in *Quantum Simulations of Complex Many-Body Systems: From Theory to Algorithms*, ed. J. Grotendorst, D. Marx and A. Muramatsu, NIC Series Vol. 10, 2002, p. 269.
11 A. B. Poma and L. Delle Site, *Phys. Rev. Lett.*, 2010, **104**, 250201.
12 L. Schulman, in *Techniques and Application of Path Integration*, John Wiley & Sons, New York, 1 edn, 1965.
13 M. Praprotnik, L. Delle Site and K. Kremer, *J. Chem. Phys.*, 2005, **123**, 224106.
14 M. Praprotnik, L. Delle Site and K. Kremer, *Phys. Rev. E: Stat., Nonlinear, Soft Matter Phys.*, 2006, **73**, 066701.
15 M. Praprotnik, K. Kremer and L. Delle Site, *Phys. Rev. E: Stat., Nonlinear, Soft Matter Phys.*, 2007, **75**, 017701.
16 M. Praprotnik, K. Kremer and L. Delle Site, *J. Phys. A: Math. Theor.*, 2007, **40**, F281.
17 L. Delle Site, *Phys. Rev. E: Stat., Nonlinear, Soft Matter Phys.*, 2007, **76**, 047701.
18 M. Praprotnik, C. Junghans, L. Delle Site and K. Kremer, *Comput. Phys. Commun.*, 2008, **179**, 51.
19 C. Junghans and S. Poblete, *Comput. Phys. Commun.*, 2010, **181**, 1449.
20 M. Praprotnik, L. Delle Site and K. Kremer, *J. Chem. Phys.*, 2007, **126**, 134902.
21 M. Praprotnik, S. Matysiak, L. Delle Site, K. Kremer and C. Clementi, *J. Phys.: Condens. Matter*, 2007, **19**, 292201.
22 S. Matysiak, C. Clementi, M. Praprotnik, K. Kremer and L. Delle Site, *J. Chem. Phys.*, 2008, **128**, 024503.
23 B. P. Lambeth, C. Junghans, K. Kremer, C. Clementi and L. Delle Site, *J. Chem. Phys.*, 2010, **133**, 221101.
24 C. Junghans, M. Praprotnik and L. Delle Site, in *Multiscale Simulation Methods in Molecular Sciences*, ed. J. Grotendorst, N. Attig, S. Blügel and D. Marx, NIC Series vol. 42, Jülich, 2009.
25 D. Reith, M. Pütz and F. Müller-Plathe, *J. Comput. Chem.*, 2003, **24**, 1624.
26 I. I. Mazin, R. J. Hemley, A. F. Goncharov, M. Hanfland and H. K. Mao, *Phys. Rev. Lett.*, 1997, **78**, 1066.
27 D. M. Ceperley and B. J. Alder, *Phys. Rev. B*, 1987, **36**, 2092.
28 T. Cui, Y. Ma and G. Zou, *J. Phys.: Condens. Matter*, 2002, **14**, 10901.
29 G. E. Ballester, D. K. Sing and F. Herbert, *Nature*, 2007, **445**, 511.
30 K. T. Delaney, C. Pierleoni and D. M. Ceperley, *Phys. Rev. Lett.*, 2006, **97**, 235702.
31 M. A. Morales, C. Pierleoni, E. Schwegler and D. M. Ceperley, *Proc. Natl. Acad. Sci. U. S. A.*, 2010, **107**, 12799.
32 D. Scharf, G. J. Martyna and M. L. Klein, *Low. Temp. Phys.*, 1993, **19**, 364.
33 K. A. Gernoth, T. Lindenau and M. L. Ristig, *Phys. Rev. B: Condens. Matter Mater. Phys.*, 2007, **75**, 174204.
34 I. F. Silvera and V. V. Goldman, *J. Chem. Phys.*, 1978, **69**, 4209.
35 M. Zoppi, M. Neumann and M. Celli, *Phys. Rev. B: Condens. Matter*, 2002, **65**, 092204.
36 Q. Wang, J. K. Johnson and J. Q. Broughton, *J. Chem. Phys.*, 1997, **107**, 5108.
37 A. Nakayama and N. Makri, *J. Chem. Phys.*, 2003, **119**, 8592.
38 J. A. Poulsen, G. Nyman and P. J. Rossky, *J. Phys. Chem. B*, 2004, **108**, 19799.
39 T. F. Miller and D. E. Manolopoulos, *J. Chem. Phys.*, 2005, **122**, 184503.
40 S. Izvekov and G. A. Voth, *J. Chem. Phys.*, 2005, **122**, 054105.
41 In fact the isotropic classical potential available in literature (introduced in the next section), if used for spherical classical particles, does not lead to the same structural properties of the liquid that one obtains by using the same potential within the path integral framework. This means that, despite the fact that the classical potential available is already simply spherical, one needs to apply in any case the coarse-graining procedure in order to get yet another isotropic potential but tuned in such a way that matches exactly the structural properties of the liquid obtained in the full path integral simulation (*cf.* also Fig. 4). This allows the structural consistency of the interfaced models. One must anyway notice that the latest methodological developments of AdResS, *via* the introduction of the thermodynamic force, allow the interface any two representations, allowing extension of the simulations to real open systems[2,42].
42 S. Poblete, S. Fritsch, C. Junghans, G. Ciccotti, L. Delle Site and K. Kremer, in preparation, 2011.
43 B. J. Berne and D. Thirumalai, *Annu. Rev. Phys. Chem.*, 1986, **37**, 401.
44 H. Wang, C. Junghans and K. Kremer, *Eur. Phys. J. E*, 2009, **28**, 221.
45 M. Cerriotti, M. Parrinello, T. E. Markland and D. E. Manolopoulos, *J. Chem. Phys.*, 2010, **133**, 124104.